NANO LETTERS

2008
Vol. 8, No. 6
1625-1630

Real Time and in Situ Control of the Gap Size of Nanoelectrodes for Molecular Devices

Dacheng Wei,[†,‡] Yunqi Liu,[*,†] Lingchao Cao,[†,‡] Yu Wang,[†,‡] Hongliang Zhang,[†,‡] and Gui Yu[†]

Beijing National Laboratory for Molecular Sciences, Institute of Chemistry, and the Graduate School, Chinese Academy of Sciences, Beijing 100080, People's Republic of China

Received January 29, 2008; Revised Manuscript Received April 3, 2008

ABSTRACT

Molecular electronics is often limited by the lack of a simple method to fabricate nanoelectrodes with controlled gap size. This is partly attributed to the lack of a real time characterization in the fabrication. Here, we report a new method based on an electron induced deposition process operated in scanning electron microscopy that realizes in situ and real time characterization in the nanoelectrode fabrication; thus the gap size can be controlled easily and precisely. It is a clean and nondestructive process for carbon nanotube (CNT) electrodes. The mechanism is detailed. The nanoelectrodes have a π-conjugated surface due to the deposition of sp^2-rich amorphous carbon. As an application, DNA molecules are assembled between the CNT electrodes by π-stacking interaction for current−voltage measurement. Our result provides a feasible route to prepare nanoelectrodes with controlled gap size, and it will be valuable for current efforts in molecular electronics and nanoelectronics.

Molecular electronics has achieved a series of significant advances in recent years;[1,2] however some problems always remain, hampering its further development. One problem is how to fabricate nanoelectrodes with controllable gap size, because as the first step to realize molecular electronics, the electrodes must be fabricated with a gap size commensurate to the size of molecules of interest.[1] Although much attention is focused there, and some successful attempts like break junction,[1] electrochemical method,[3] and nanowire lithography[4] have been reported, the precise control of the gap size and other difficulties still need be resolved. For instance, it is a problem to provide a real time characterization in the fabrication of the nanoelectrodes; thus the exact gap size is usually undetectable in the fabrication and then the precise control of the gap size would be unfeasible and inefficient. Moreover, the existing methods often are far routine, low yielding, hard to implement. Here, we develop a simple and efficient method to fabricate nanoelectrodes with a traditional scanning electron microscope, which can not only induce the formation of nanogaps but also provide an in situ and real time characterization in the fabrication. So we can control the gap size more easily and precisely compared with the present methods. As an example, carbon nanotube (CNT) electrodes with various nanogap sizes are fabricated, and then DNA molecules are connected between these CNT electrodes via a new route based on a self-assembly process, and the electrical measurement shows good contact via $\pi-\pi$ stacking.

The conventional electrodes for molecular devices are metal electrodes such as atomic force microscopy (AFM) tips, gold nanoelectrodes, etc. As another choice, the use of CNTs as the electrode for molecular devices has received increasing attention in recent years.[5–7] In these works, CNT electrodes are fabricated via a strategy of cutting a CNT by focused-ion-beam etching (FIB),[5] current breakdown,[6] or local plasma ablation method[7] and then leaving the two ends separated by a nanogap. Compared with metal electrodes, CNTs show higher conductivity,[8,9] lower screening of the gate electric fields by the source/drain electrodes for their smaller size,[6] and better contact with organic molecules,[7] so they have been regarded as an ideal material for molecular electrodes. In our research, multiwalled CNTs (MWCNTs) are mainly used, because the MWCNTs are reliable for use as electrodes. About two-thirds of single-walled CNTs (SWCNTs) are semiconductive; while almost all MWCNTs are metallic with high conductivity at room temperature,[8,9] although a very small band gap (tens of millielectronvolts) is present.[10] Moreover, MWCNTs favor ohmic contact[10] and can bear large current.[9]

* Author to whom correspondence should be addressed. Tel.: +86-10-62613253. Fax: +86-10-62559373 . E-mail: liuyq@mail.iccas.ac.cn.
† Beijing National Laboratory for Molecular Sciences, Institute of Chemistry.
‡ Graduate School.

10.1021/nl080283+ CCC: $40.75
Published on Web 05/23/2008

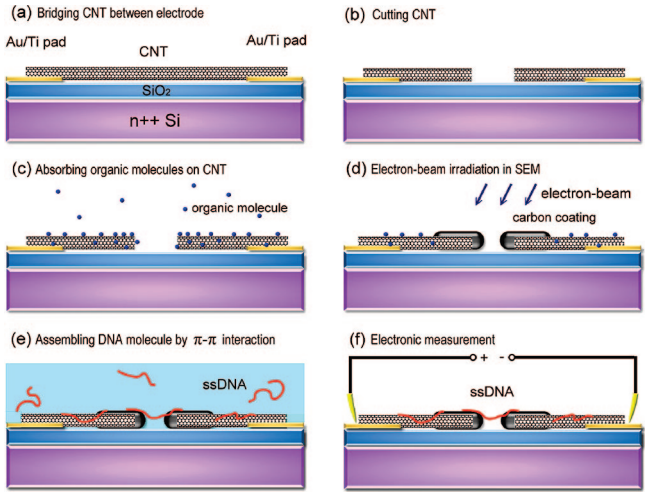

Figure 1. Schematic diagram of the process of the fabrication of a CNT electrode with a controlled nanogap (a−d) and the fabrication of a DNA electronic device (e, f). (a) Bridging a CNT between Au/Ti electrodes. (b) Cutting the CNT by current breakdown method. (c) Adsorbing organic molecules on or in the CNT. (d) Irradiating the gap of the CNT by electron beam with in situ observation in SEM. (e) Assembling DNA molecules between the CNT electrodes by immerging in DNA buffer solution. (f) Measuring the electronic properties of the bridged DNA molecules.

The procedure for fabricating the CNT electrode is illustrated in Figure 1a−d. MWCNTs (Figure S1) used here were produced by a chemical vapor deposition method described elsewhere.[11] They were perfectly graphitic in nature. SWCNTs (Figure S2) were synthesized by catalytic decomposition of ethanol as described in ref 12. For the first step, a CNT is placed between Au/Ti electrodes on a SiO_2/Si wafer. For the second step, a wide original gap is prepared by cutting it at the middle via an existing method, such as FIB, current breakdown, or local plasma ablation. Here, we use the current breakdown method as described in ref 6 and get original gaps normally in the range of 10−60 nm. As it is complicated and difficult to obtain tiny gaps (less than 10 nm) with precise size by these methods, these original gaps need to be further treated by the following procedures. For the third step, the electrode is exposed to organic vapor (here toluene or ethanol is used) to absorb organic molecules in the cavity or on the surface of the CNT. For the final step, the electrode with an original gap is placed in a scanning electron microscope (operated at 15 kV). With large magnification, a high-density electron beam is obtained, focusing on the area of the gap of the electrode. Figure 2a shows the irradiation process. After the current breakdown process, an original MWCNT with a diameter of 33 nm forms a ca. 25 nm gap. By irradiation with an electron density of 2×10^7 A/m^2, the irradiated part of the MWCNT gradually becomes broader, and as a result the gap becomes narrower. After 6 min, the diameter of the MWCNT increases to ca. 49 nm, while the gap decreases to ca. 4 nm. Finally, after 10 min, the gap disappears, and two ends of the MWCNT are connected. This process is observed in real time and in situ by SEM, so we can stop the process at any time, and then a CNT electrode with the gap size corresponding to our need is obtained. It is a simple and efficient method. By this method, MWCNT electrodes with a series of gap sizes are fabricated as shown in Figure 2b.

In previous research, the SEM serves primarily as a tool to precisely characterize the gap size of the nanoelectrodes;[3,4] while in this method, the scanning electron microscope plays two roles. First, the scanning electron microscope provides an in situ and real time characterization of the gap size, making it feasible to control the gap size. Second, the electron beam induces broadening of CNTs and narrowing of the gap. This broadening effect is also detected by atomic force microscopy (AFM) characterization (Figure 3a). After irradiation, the height of the MWCNT around the gap increases from 47.2 to 60.1 nm, indicating a deposition on MWCNT, while no observable changes of the height are detected on the substrate, indicating the deposition just takes place on the MWCNT surface but rare on the substrate. We also examine the Raman spectra of a MWCNT (Figure 3b). After irradiation, the peaks centered at 1339 and 1590 cm^{-1}, which corresponds to D-band and G-band of MWCNT, do not shift obviously, thus suggesting it is a nondestructive process for MWCNT. Two new peaks centered at 1335 and 1530 cm^{-1} are observed, corresponding to the D-band and G-band of amorphous carbon (a-C), respectively. The D-band, which is related to the breathing mode of aromatic carbon, only occurs in the sp^2 carbon with small cluster size;[13] thus the existence of a D-band indicates that the sp^2 carbon exists in the a-C, while the high ratio between the intensity of the D-band and G-band (I_D/I_G) indicates the small sp^2 cluster size and the high content of the sp^2 carbon in the a-C.[14,15] The a-C is not possible to be sp^3 rich carbon, since in the case of high sp^3 content a-C, the I_D/I_G will tend to zero,[15] and there is not an obvious peak around 1180 cm^{-1}, which originates from the sp^3 carbon.[15,16] Hence, the a-C is rich with conductive sp^2 carbon clusters,[17] corresponding with the transmission electron microscopy (TEM) observation by Banhart.[18] The a-C would not come from the destruction of the MWCNT, thus indicating a foreign deposition of a-C, and an irradiation-induced graphitization would be integrated into the deposition process when carried out at sufficient electron energy.[18] Furthermore, as a control experiment, we did not expose the MWCNT electrode in organic vapor but dried it in an oven at 120 °C for 48 h to remove the absorbed organic molecules before the irradiation process. After 6 min of irradiation, the diameter and the gap size of the MWCNT electrodes changed a little (Figure S3); thus the deposition would come from the electron beam induced decomposition (EBID) of the absorbed organic molecules, and the deposition induced by the pump oil in the scanning electron microscope chamber could be ignored. Therefore, the broadening effect should be attributed to the EBID process. EBID is a maskless process using a high-intensity electron beam to deposit nanoscale structures on a scanned surface, and it has been used to connect CNTs in previous work.[18] In our case, complex beam-induced reactions of organic molecules occur when the electron beam is focused to the CNT electrode, leading to the decomposition of these organic molecules into a-C for deposition. The EBID process would just take place on the CNTs. The organic molecules favor to physically

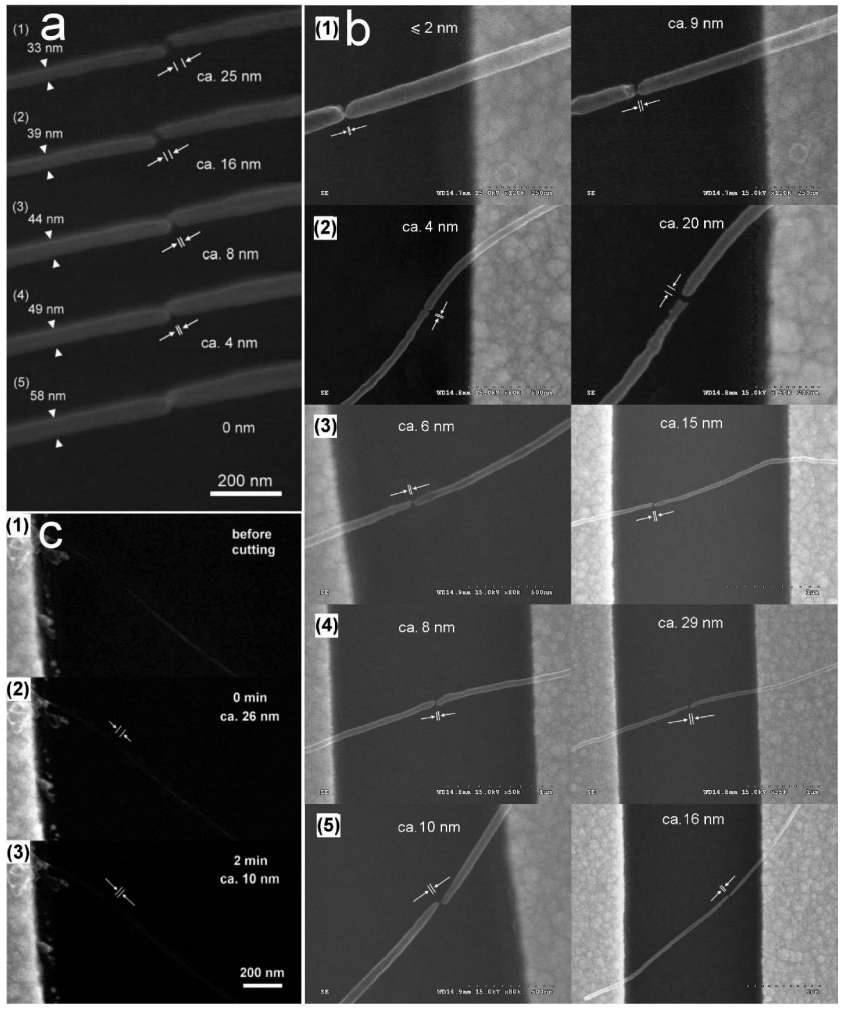

Figure 2. (a) SEM images of the MWCNT electrode in the EBID process: (1) just after current breakdown; (2−5) after an EBID process of 2, 4, 6, and 10 min, respectively. (b) MWCNT electrodes with a series of gap sizes fabricated by the EBID method: (1−5) The left images are SEM images measured after the EBID process, the gap sizes are ca. 2, 4, 6, 8, and 10 nm, respectively, and the right images are SEM images measured before the EBID process. (c) SEM images of a nanoelectrode which is made of a small bundle of SWCNTs (1) before current breakdown, (2) before the EBID process, and (3) after about 2 min in the EBID process.

absorb inside or outside of the CNTs due to their strong interactions with the sidewalls of the CNTs; thus many groups reported the CNTs could be used as the gas sensors, or be encapsulated, noncovalently functionalized with organic molecules.[19–21] The aromatic molecules like toluene can absorb on the sp^2 CNT sidewalls due to a strong π-stacking interaction,[19] while ethanol can also be adsorbed effectively.[20] Therefore, most of absorbed organic molecules exist on the CNTs; thus in the irradiation, the absorbed molecules decompose and then immobilize on the CNT surface, causing broadening of the diameter and reduction of the gap size. Although there would be a small amount of molecules absorbed on the substrate, they can also be easily pumped out from the SEM chamber due to the weak interaction with the substrate; thus in AFM image (Figure 3a), the nonobservable deposition of a-C can be observed on the substrate. Moreover, we could also assume another possibility that the sp^2-rich a-C would tend to deposit on the CNTs instead of on the substrate due to the π-stacking interaction.

As we know, the strong electron beam can change, destroy, or collapse the structure of CNTs, and then the electrical properties will be dramatically changed;[22] however there exists a threshold electron energy.[23] Below this threshold electron energy, CNTs cannot be destroyed. The threshold electron energy is approximately 100 keV for MWCNTs and 86 keV for SWCNTs.[23,24] In our research, the SEM provides an electron beam with an appropriate energy in the process. The accelerating voltage is only 15 kV, so it is weak enough to avoid the destruction of the CNTs, but strong enough to induce the EBID. Furthermore, the electron beam irradiation is a clean process without introducing impure atoms as well as a nondestructive process for the CNTs, thus the electrical properties are not obviously changed and the current−voltage ($I-V$) curves of a MWCNT (Figure S4) show a similar behavior before and after the EBID process.

We examined electrical properties of a MWCNT electrode in the fabrication. Figure 3c shows the $I-V$ curves measured before (line 1) and after current breakdown (line 2), when a 4 nm gap forms in the EBID process (line 3), and finally when the gap disappears (line 4). Before current breakdown, the $I-V$ curve (line 1) is linear, indicating the MWCNT is well contacted with the Au/Ti electrodes. Line 3 shows a

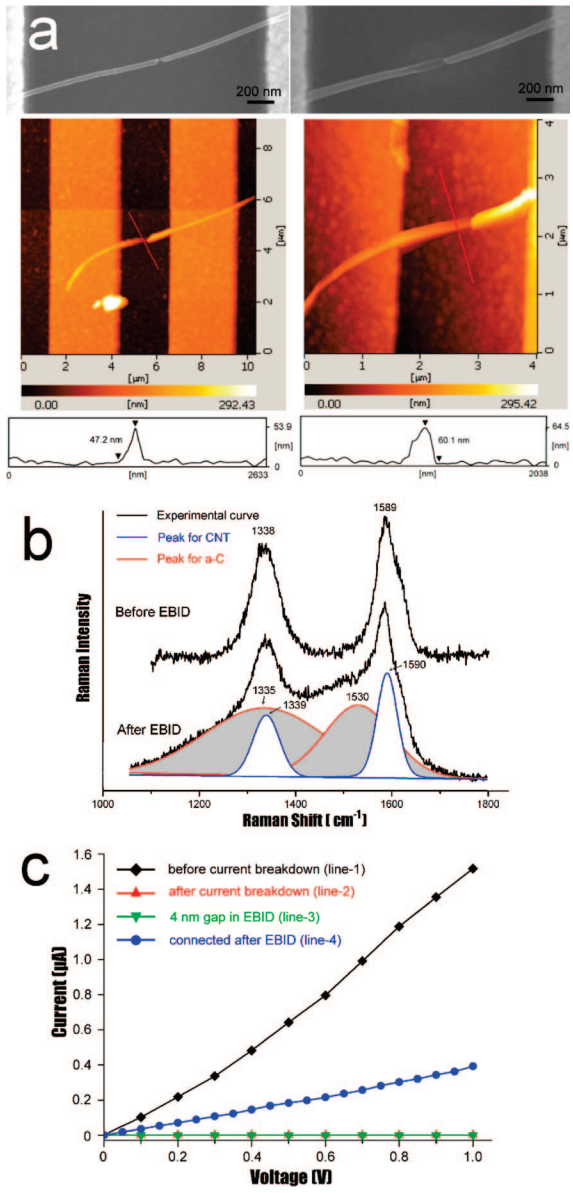

Figure 3. (a) SEM and AFM images of a MWCNT electrode before (left figures) and after (right figures) the EBID process. The bottoms are the topography height profiles along the red lines in the AFM images. (b) Raman spectra of a MWCNT before and after the EBID process. After the EBID process, the peaks for MWCNT (white Lorentzians) are unchanged, suggesting a nondestructive process for the MWCNT, while two new peaks (gray Lorentzians) appear, corresponding to the deposited a-C. (c) $I-V$ curves of the CNT electrode before current breakdown (black), after current breakdown (red), when a 4 nm gap formed in the EBID process (green), and when connected after the EBID process (blue).

similar behavior with line 2, that the current is down to the noise limit of the measurement, indicating no impurity is deposited into the gap in the EBID process. When two ends of the MWCNT are connected by a-C (line 4), a considerable current is observed. This result shows the deposited a-C is conductive, and if we further graphitize the a-C by thermal or current annealed, a better conduction could be obtained.

We have also successfully fabricated nanoelectrodes by using SWCNTs as the material of the electrodes. In contrast to MWCNTs, SWCNTs have smaller diameter; thus devices

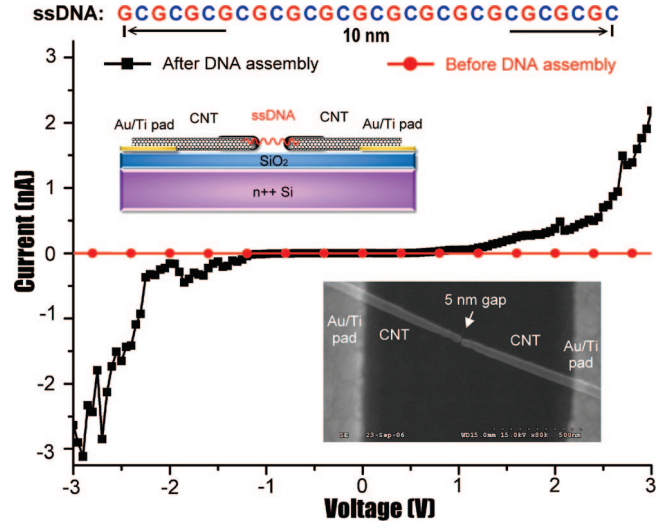

Figure 4. The electrical properties of a DNA device fabricated by using the MWCNT electrodes. The $I-V$ curves are measured before (red) and after (black) the assembly of DNA on the MWCNT nanoelectrode. The upper inset shows a scheme of the device, and the lower inset is the SEM image of a MWCNT nanoelectrode used in the device.

with higher integration density can be fabricated. The fabrication procedure is similar to that of nanoelectrodes of MWCNTs. An original gap is formed by current breakdown of a small bundle of SWCNTs, and after about a 2 min EBID process, the gap decreases from ca. 26 nm to ca. 10 nm as shown in Figure 2c. Moreover, this method would have the potential to fabricate nanoelectrodes made of other materials and then produce nanoelectrodes with a controlled gap and a π-conjugated surface which is rich in sp^2 carbon clusters.

Finally, as an application, DNA devices are fabricated by using the MWCNT electrodes. DNA is a naturally occurring polymer that plays a central role in biology. In previous research, DNA molecules have been connected in circuit by Au nanogap electrodes or SPM tips via an electrostatic trapping or a bonding process, and the current flows through the electrode/DNA interface by tunneling barriers or Au/S bond.[25,26] Here, we connect DNA molecules in the circuit by another route, which is illustrated in Figure 1e,f. We used 10 nm long poly(GC) single-stranded DNA (ssDNA) oligomers (GCG CGC GCG CGC GCG CGC GCG CGC GCG CGC), and used two types of MWCNT electrodes. One (EL-1) was with a gap larger than 10 nm without the EBID process, the other (EL-2) was treated by an EBID process with a ca. 5 nm gap. The MWCNT electrodes were immersed into the solution of DNA, and then the DNA molecules would assemble between the MWCNT electrodes. Figure 4 shows the electrical properties after the assembly process. We fabricated more than 30 devices by using EL-1; no DNA molecules were bridged. This is because the electrodes have a larger gap size than the length of the DNA. About 15% of the EL-2 were bridged by one or several DNA molecules, and typical $I-V$ curves of DNA molecules were observed, whose current was essentially zero at low bias, while beyond a threshold bias the current rose sharply. This behavior is similar to previous work where measurement were obtained by using Au nanogap electrodes or SPM tips,[25,26] indicating

that the DNA molecules are assembled between the electrodes and the charge transport between the MWCNT electrodes and DNA is also efficient. We assume it would go through a π-stacking assembly process. The ssDNA has exposed aromatic bases; a very strong π-stacking interaction exists between the bases of ssDNA and the side-wall of CNTs or other aromatic materials like sp^2-rich a-C.[27–29] Thus the ssDNA shows much stronger interaction than double-stranded DNA;[29,30] the bases are extended from the backbone and stack onto the π-conjugated surface, causing the wrapping of ssDNA on the electrode.[28] Then, the hybridization of the bridged ssDNA would take place, forming a conductive duplex structure. The π-stacking between the MWCNT electrodes and DNA can provide a well contact,[31] while the π-stacking between the conjugated base pairs in hybridized DNA enables charge transport over long distance, thus DNA has significant potential applications in molecular electronics.[32] Several mechanisms have been suggested for the charge transport in DNA.[25,33–35] In our case, the charge transport may be through a hopping mechanism, in which the charge sequentially hops between the adjacent base pairs.[35] The band transport mechanism is also possible, in which π-stacking interaction between bases leads to a molecular band where the electronic states are delocalized over the entire length of DNA.[25] For both mechanisms, the charge injects when the Fermi level of the electrode is aligned with the band edge by applying the bias voltage, and then charge transport occurs through hopping or band conduction. Thus a sharp rise of current was observed at a threshold bias.[25]

In conclusion, nanoelectrodes with a controllable nanogap size are fabricated by an EBID method. In the process, the SEM provides an electron beam with appropriate energy, which can induce the EBID to decrease the gap size of the CNT electrode while avoiding the destruction of the CNTs, and an in situ and real time characterization, which makes it relatively feasible and facile to control the nanogap size in a relatively precise manner. Due to its controllability, wide ranges of nanogaps can be prepared for various molecules or nanomaterials, and it is also a compatible process to current microelectronics. Thus it would be valuable for the current efforts to investigate or realize molecular electronics or nanoelectronics. Moreover, after the EBID process, a π-conjugated surface forms due to the deposition of sp^2-rich a-C; thus we can connect π-conjugated molecules like DNA between these electrodes by π-stacking interaction, offering another choice to connect molecules in a circuit.

Acknowledgment. We thank Dr. H. M. Liu and Professor X. Y. Liu (Institute of Microelectronics, Chinese Academy of Sciences). This work was supported by the Major State Basic Research Development Program, the National Natural Science Foundation of China (50673093, 60671047, 60736004, 20721061, 20573115), and the Chinese Academy of Sciences.

Supporting Information Available: The detailed description of the experiment and supporting Figures S1 (TEM images of MWCNTs), S2 (TEM and SEM images of SWCNTs), S3 (SEM images of the EBID process of a dried MWCNT electrode), and S4 ($I-V$ curves of a MWCNT after the EBID process). This material is available free of charge via the Internet at http://pubs.acs.org.

References

(1) Reed, M. A.; Zhou, C.; Muller, C. J.; Burgin, T. P.; Tour, J. M. *Science* **1997**, *278*, 252–254.
(2) (a) Joachim, C.; Gimzewski, J. K.; Aviram, A. *Nature* **2000**, *408*, 541–548. (b) Dadosh, T.; Gordin, Y.; Krahne, R.; Khivrich, I.; Mahalu, D.; Frydman, V.; Sperling, J.; Yacoby, A.; Joseph, I. B. *Nature* **2005**, *436*, 677–678.
(3) Qing, Q.; Chen, F.; Li, P.; Tang, W. H.; Wu, Z. Y.; Liu, Z. F. *Angew. Chem., Int. Ed.* **2005**, *44*, 7771–7775.
(4) (a) Qin, L. D.; Park, S. H.; Huang, L.; Mirkin, C. A. *Science* **2005**, *309*, 113–115. (b) Liu, S. H.; Tok, J. B. H.; Bao, Z. N. *Nano Lett.* **2005**, *5*, 1071–1076. (c) Qin, L. D.; Jang, J. W.; Huang, L.; Mirkin, C. A. *Small* **2007**, *3*, 86–90.
(5) Horiuchi, K.; Kato, T.; Hashii, S.; Hashimoto, A.; Sasaki, T.; Aoki, N.; Ochiai, Y. *Appl. Phys. Lett.* **2005**, *86*, 153108.
(6) Qi, P.; Javey, A.; Rolandi, M.; Wang, Q.; Yenilmez, E.; Dai, H. J. *J. Am. Chem. Soc.* **2004**, *126*, 11774–11775.
(7) (a) Guo, X. F.; Small, J. P.; Klare, J. E.; Wang, Y.; Purewal, M. S.; Tam, I. W.; Hong, B. H.; Caldwell, R.; Huang, L.; O'Brien, S.; Yan, J. M.; Breslow, R.; Wind, S. J.; Hone, J.; Kim, P.; Nuckolls, C. *Science* **2006**, *311*, 356–359. (b) Guo, X. F.; Myers, M.; Xiao, S.; Lefenfeld, M.; Steiner, R.; Tulevski, G. S.; Tang, J. Y.; Baumert, J.; Leibfarth, F.; Yardley, J. T.; Steigerwald, M. L.; Kim, P.; Nuckolls, C. *Proc. Natl. Acad. Sci. U.S.A.* **2006**, *103*, 11452–11456.
(8) Frank, S.; Poncharal, P.; Wang, Z. L.; Heer, W. A. D. *Science* **1998**, *280*, 1744–1746.
(9) Li, H. J.; Lu, W. G.; Li, J. J.; Bai, X. D.; Gu, C. Z. *Phys. Rev. Lett.* **2005**, *95*, 086601.
(10) Dresselhaus, M. S.; Dresselhaus, G.; Avouris, P. *Carbon Nanotubes, Topics of Applied Physics*; Springer-Verlag: Berlin, 2001; 329-390.
(11) Wang, X. B.; Liu, Y. Q.; Zhu, D. B. *Adv. Mater.* **2002**, *14*, 165–167.
(12) Wang, Y.; Liu, Y. Q.; Wei, D. C.; Cao, L. C.; Fu, L.; Li, X. L.; Kajiura, H.; Li, Y. M.; Noda, K. *J. Mater. Chem.* **2007**, *17*, 357–363.
(13) Thomsen, C.; Reich, S. *Phys. Rev. Lett.* **2000**, *85*, 5214–5217.
(14) (a) Ferrari, A. C.; Robertson, J. *Phys. Rev. B* **2000**, *61*, 14095. (b) Baptista, D. L.; Zawislak, F. C. *Diamond Relat. Mater.* **2004**, *13*, 1791 1801. (c) Fazio, E.; Barletta, E.; Barreca, F.; Mondio, G.; Neri, F.; Trusso, S. Laser Ablation-Deposited CN_x Thin Films. In *Carbon: The Future Material for Advanced Technology Applications*; Messina, G., Santangelo, S., Eds.; Springer-Verlag: Berlin, 2006; pp 287−302.
(15) Schwan, J.; Ulrich, S.; Batori, V.; Ehrhardt, H. Silva, S. R. P. *J. Appl. Phys.* **1996**, *80*, 440–447.
(16) Shroder, R.; Nemanich, R.; Glass, J. *Phys. Rev. B* **1990**, *41*, 3738–3745.
(17) (a) Baptista, D. L.; Zawislak, F. C. *Diamond Relat. Mater.* **2004**, *13*, 1791–1801. (b) Ferrari, A. C.; Robertson, J. *Phys. Rev. B* **2000**, *61*, 14095–14107.
(18) Banhart, R. *Nano Lett.* **2001**, *1*, 329–332.
(19) (a) Kondratyuk, P.; Yates, J. T. *Acc. Chem. Res.* **2007**, *40*, 995–1004. (b) Tournus, F.; Latil, S.; Heggie, M. I.; Charlier, J. C. *Phys. Rev. B* **2005**, *72*, 075431. (c) Chen, R. J.; Zhang, Y. G.; Wang, D. W.; Dai, H. J. *J. Am. Chem. Soc.* **2001**, *123*, 3838–3839. (d) Takenobu, T.; Takano, T.; Shiraishi, M.; Murakami, Y.; Ata, M.; Kataura, H.; Achiba, Y.; Iwasa, Y. *Nat. Mater.* **2003**, *2*, 683–688.
(20) Nisha, J. A.; Yudasaka, M.; Bandow, S.; Kokai, F.; Takahashi, K.; Iijima, S. *Chem. Phys. Lett.* **2000**, *328*, 381–386.
(21) (a) Kong, J.; Franklin, N. R.; Zhou, C. W.; Chapline, M. G.; Peng, S.; Cho, K.; Dai, H. J. *Science* **2000**, *287*, 622–625. (b) Li, J.; Lu, Y. J.; Ye, Q.; Cinke, M.; Han, J.; Meyyappan, M. *Nano Lett.* **2003**, *3*, 929–933.
(22) An, K. H.; Park, K. A.; Heo, J. G.; Lee, J. Y.; Jeon, K. K.; Lim, S. C.; Yang, C. W.; Lee, Y. S.; Lee, Y. H. *J. Am. Chem. Soc.* **2003**, *125*, 3057–3061.
(23) (a) Banhart, F.; Li, J. X.; Terrones, M. *Small* **2005**, *1*, 953–956. (b) Banhart, F. *Rep. Prog. Phys.* **1999**, *62*, 1181–1221.
(24) Smith, B. W.; Luzzi, D. E. *J. Appl. Phys.* **2001**, *90*, 3509–3515.
(25) Porath, D.; Bezryadin, A.; Vries, S. D.; Dekker, C. *Nature* **2000**, *403*, 635–638.
(26) Cohen, H.; Nogues, C.; Naaman, R.; Porath, D. *Proc. Natl. Acad. Sci. U.S.A.* **2005**, *102*, 11589–11593.
(27) Gao, H. J.; Kong, Y. *Annu. Rev. Mater. Res.* **2004**, *34*, 123–150.

(28) (a) Zheng, M.; Jagota, A.; Strano, M. S.; Santos, A. P.; Barone, P.; Chou, S. G.; Diner, B. A.; Dresselhaus, M. S.; Mclean, R. S.; Onoa, G. B.; Samsonidze, G. G.; Semke, E. D.; Usrey, M.; Walls, D. J. *Science* **2003**, *302*, 1545–1548. (b) Zheng, M.; Jagota, A.; Semke, E. D.; Diner, B. A.; Mclean, R. S.; Lustig, S. R.; Richardson, R. E.; Tassi, N. G. *Nat. Mater.* **2003**, *2*, 338–342.
(29) Zhao, X. C.; Johnson, J. K. *J. Am. Chem. Soc.* **2007**, *129*, 10438–10445.
(30) Pividori, M. I.; Alegret, S. *Top. Curr. Chem.* **2005**, *260*, 1–36.
(31) Lu, G.; Maragakis, P.; Kaxiras, E. *Nano Lett.* **2005**, *5*, 897–900.
(32) Bhalla, V.; Bajpai, R. P.; Bharadwaj, L. M. *EMBO Rep.* **2003**, *4*, 442–445.
(33) Berlin, Y. A.; Burin, A. L.; Ratner, M. A. *J. Am. Chem. Soc.* **2001**, *123*, 260–268.
(34) Giese, B.; Amaudrut, J.; Kohler, A. K.; Spormann, M.; Wessely, S. *Nature* **2001**, *412*, 318–320.
(35) (a) Giese, B. *Acc. Chem. Res.* **2000**, *33*, 631–636. (b) Bixon, M.; Giese, B.; Wessely, S.; Langenbacher, T.; Michel-Beyerle, M. E.; Jortner, J. *Proc. Natl. Acad. Sci. U.S.A.* **1999**, *96*, 11713–11716.

NL080283+